Available online at www.sciencedirect.com
ScienceDirect
Applied Catalysis B: Environmental 79 (2008) 26–34
APPLIED CATALYSIS B: ENVIRONMENTAL
www.elsevier.com/locate/apcatb

Mesoporous CuO–Fe_2O_3 composite catalysts for low-temperature carbon monoxide oxidation

Jian-Liang Cao, Yan Wang, Xiu-Ling Yu, Shu-Rong Wang, Shi-Hua Wu, Zhong-Yong Yuan *

College of Chemistry, Nankai University, Tianjin 300071, PR China

Received 8 August 2007; received in revised form 4 October 2007; accepted 5 October 2007
Available online 11 October 2007

Abstract

A series of mesoporous CuO–Fe_2O_3 composite oxide catalysts with different CuO contents were prepared by a surfactant-assisted method of nanoparticle assembly. The prepared composite oxides were characterized by X-ray diffraction, N_2 adsorption, transmission electron microscopy, hydrogen temperature-programmed reduction, thermogravimetry–differential thermal analysis and X-ray photoelectron spectroscopy. Their catalytic behavior for low-temperature CO oxidation was studied by using a microreactor-GC system. These mesoporous CuO–Fe_2O_3 catalysts possess a wormhole-like mesostructure with a narrow pore size distribution and high surface area, exhibiting high catalytic activity and stability for low-temperature CO oxidation. The catalytic behavior depended on the CuO content, the precalcination temperature, the surface area and the particle size of the catalysts. The catalyst with 15 mol% CuO content and calcined at 300 °C exhibited the highest catalytic activity and stability.

Keywords: CuO–Fe_2O_3 catalyst; Mesoporous; CO oxidation; Catalytic activity

1. Introduction

Because of the physical and chemical properties of materials depend not only on the chemical composition but crucially also on their porosity and shape [1], much effort has been focused on tailoring the pore size and external morphology of the materials [2–5]. In a supported catalyst system, mesoporous oxides have recently attracted great interest for the use as catalyst and catalyst supports [6–8], since the mesoporous supports have remarkably large surface areas and narrow pore size distributions so as to give rise to well dispersed and stable metal particles on the surface and as consequence would show an improved catalytic performance.

Iron oxides are of technological importance as catalytic materials, sorbents, pigments, flocculents, coatings, gas sensors and ion exchangers [9–14]. Iron oxide-based catalysts have been found to be good candidates as cheap and efficient catalysts, especially in environmental catalysis. Due to the dual functions of iron oxide as a catalyst of carbon monoxide in the presence of oxygen, and in the absence of oxygen, as a direct carbon oxide oxidant by losing the lattice oxygen, iron oxide-based catalysts are attractive candidates amongst the readily available carbon monoxide oxidation catalysts especially in the removal of carbon monoxide in a burning cigarette, where the potential toxicity of other catalysts would be undesirable. Haruta et al. [15,16] firstly demonstrated active Au/Fe_2O_3 catalysts for room temperature CO oxidation. Both heat-treated and untreated Au/Fe_2O_3 catalysts were found to exhibit low-temperature activity toward CO oxidation, with untreated samples being much more active, though the heat-treatment could control the catalytic activity for CO oxidation [17–21]. The deposition–precipitation method was shown to produce more active Au/Fe_2O_3 catalysts than conventional coprecipitation [19,22]. Hutchings and co-workers [23] prepared an Au/Fe_2O_3 catalyst using a two-stage calcinations procedure for the competitive oxidation of dilute CO in the presence of moist excess H_2 and CO_2, achieving target conversion and selectivity. Although iron oxides supported precious metal catalysts have been demonstrated to be very effective for low-temperature CO oxidation, the high cost and limited availability discourage the

* Corresponding author. Tel.: +86 22 23509610; fax: +86 22 23509610.
E-mail address: zyyuan@nankai.edu.cn (Z.-Y. Yuan).

0926-3373/$ – see front matter © 2007 Elsevier B.V. All rights reserved.
doi:10.1016/j.apcatb.2007.10.005

applications of precious metal catalysts, and transition metals and oxides such as copper oxides are significant to be explored as an alternative catalytic component to reduce using or even replace the precious metal base catalysts [24,25]. The reported copper iron composite oxide catalysts were prepared by coprecipitation, ball-milling, thermal solid–solid interaction, and sol–gel method [26–30], and few were studied on low-temperature CO oxidation. It is still a challenge to develop high surface area and porous CuO–Fe_2O_3 composite materials for the anticipation of enhancing catalytic performance.

Herein, we report a surfactant-assisted method for preparing mesoporous CuO–Fe_2O_3 composite oxide catalysts with high surface area. The resulting mesoporous CuO–Fe_2O_3 composite oxides show high catalytic activity on the low-temperature carbon monoxide oxidation. The influence of CuO content and calcination temperature on the catalytic performance of the catalysts is investigated systematically.

2. Experimental

2.1. Catalyst preparation

All chemicals were used as received without further purification. In a typical synthesis procedure of the mesoporous CuO–Fe_2O_3 composite catalysts with different CuO content, 6 mmol cetyltrimethylammonium bromide was dissolved into 200 ml distilled water at room temperature, followed by ultrasound irradiation 15 min. Then 10 mmol $Fe(NO_3)_3{\cdot}6H_2O$ and calculated amount of $Cu(NO_3)_2{\cdot}3H_2O$ were added into the above solution under magnetic stirring. After stirring for 0.5 h, 0.2 mol/l sodium hydroxide solution was gradually added until the pH value of the mixed solution was 9. The final suspended solution was aged at 90 °C for 3 h. The precipitate was filtered, washed with hot water, dried in the oven at 110 °C for 12 h, then milled and calcined at 300 °C for 5 h. The nominal content of CuO was 10, 15, 20, 25, 33 and 50 mol%, and the corresponding catalysts were denoted as FeCu10, FeCu15, FeCu20, FeCu25, FeCu33 and FeCu50, respectively. The actual composition of the catalyst was analyzed by inductively coupled plasma emission spectroscopy (ICP), and listed in Table 1, which shows that the actual CuO content was a little higher than the nominal CuO content in the starting solution.

Table 1
Nominal and actual composition and content (molar fraction) of the prepared CuO–Fe_2O_3 composite oxides

Catalyst	Nominal composition		Actual composition (from ICP)			
	Cu (mol%)	Fe (mol%)	Cu (wt%)	Cu (mol%)	Fe (wt%)	Fe (mol%)
FeCu10	10	90	6.98	10.73	51.02	89.27
FeCu15	15	85	10.29	16.43	45.99	83.57
FeCu20	20	80	14.14	22.25	43.42	77.75
FeCu25	25	75	17.58	26.89	42.00	73.11
FeCu33	33	67	23.68	35.57	37.69	64.43
FeCu50	50	50	36.18	52.28	29.02	47.72

The relative uncertainty in the ICP results is ±5%.

2.2. Characterization

X-ray diffraction (XRD) analysis was performed on a Rigaku D/max-2500 diffractometer, with Cu Kα radiation at 40 kV and 100 mA in a scanning range of 3–80° (2θ). The diffraction peaks of the crystalline phase were compared with those of standard compounds reported in the JCPDS Date File.

Nitrogen adsorption–desorption isotherms were collected at liquid nitrogen temperature using a Quantachrome NOVA 2000e sorption analyzer. The specific surface areas (S_{BET}) of the samples were calculated following the multi-point BET (Brunauer–Emmett–Teller) procedure. The pore-size distributions were determined from the adsorption branch of the isotherms using the BJH (Barett–Joyner–Halenda) method. Before carrying out the measurement, each sample was degassed at 200 °C for more than 6 h.

Transmission electron microscopy (TEM) analysis was performed on a Philips Tecnai G20 microscope, operating at 200 kV. The sample was dispersed in ethanol and treated with ultrasound for 5 min, and then deposited on a copper grid coated with preformed holey carbon film.

The chemical composition of the sample was analyzed by inductively coupled plasma emission spectroscopy (ICP) on a ICP-9000 (N + M) spectrometer made by USA Thermo Jarrell-Ash Corp.

The reducibility of CuO–Fe_2O_3 catalysts was measured by hydrogen temperature-programmed reduction (H_2-TPR). The experiments were performed under the mixture of 5% H_2 in N_2 flowing (30 ml/min) over 50 mg of catalyst at a heating rate of 10 °C/min. The uptake amount during the reduction was measured by using a thermal conductivity detector (TCD). For comparison, H_2-TPR measurement of pure CuO was carried out over 4.6 mg of CuO powder.

Thermogravimetry–differential thermal analysis (TG–DTA) of the sample was conducted on a Rigaku Standard Model thermal analyzer in air atmosphere (flow rate: 90 ml/min and heat rate: 10 °C/min).

X-ray photoelectron spectroscopy (XPS) measurements were carried out on a PHI 5300 system spectrophotometer with the Mg Kα radiation. The operating conditions were kept constantly at 187.5 eV and 250.0 W. In order to subtract the surface charging effect, the C1s peak has been fixed at a binding energy of 284.6 eV.

2.3. Catalytic activity test

Catalytic activity and stability tests were performed in a continuous-flow fixed-bed microreactor at atmospheric pressure. A stainless steel tube with an inner diameter of 7 mm was chosen as the reactor tube. About 200 mg catalyst power was placed into the tube. The reaction gas mixture consisting of 10 vol.% CO balanced with air was passed through the catalyst bed at a total flow rate of 36.6 ml/min. A typical weigh hourly space velocity (WHSV) was 11,000 ml/(h g). After 30 min reaction, the effluent gases were analyzed online by a GC-900A gas chromatograph equipped with a thermal conductivity detector (TCD). The activity was expressed by the conversion of CO.

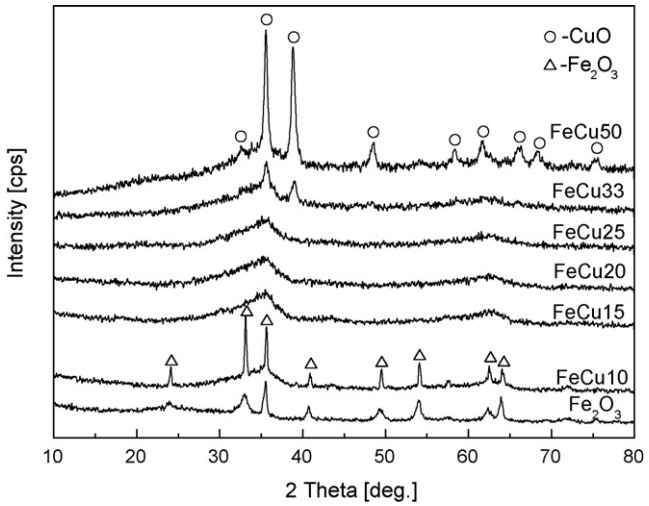

Fig. 1. XRD patterns of the prepared CuO–Fe_2O_3 composite oxides with different CuO contents calcined at 300 °C.

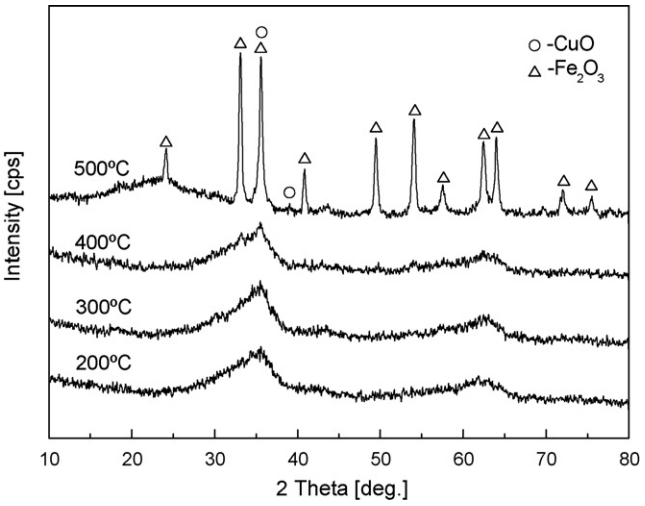

Fig. 2. XRD patterns of FeCu15 samples calcined at different temperatures.

3. Results and discussion

3.1. Catalyst characterization

Fig. 1 shows the XRD patterns of the surfactant-prepared CuO–Fe_2O_3 composite oxides with different CuO contents after calcination at 300 °C. The FeCu10 sample presents only the reflections characteristic of rhombohedral hematite Fe_2O_3 structure, without any other impure phases. Compared with the diffraction pattern of the pure Fe_2O_3 prepared by the same procedure, the (1 0 4) and (1 1 0) peaks shift from 32.94° and 35.54° to 33.14° and 35.64° (2θ) for the FeCu10 sample synthesized with the 10% content of CuO, respectively. This indicates the change of the lattice parameters after the synthesis with 10% content of CuO, suggesting the incorporation of small quantity of Cu species into the lattice of hematite Fe_2O_3 to form solid solution and/or the interaction between CuO and Fe_2O_3 when high dispersion of the CuO nanoparticles with very small particle sizes on the surface of Fe_2O_3. When the CuO content is in the range of 15–25 mol%, the corresponding samples are amorphous. Further increase of the CuO content into 33 and 50 mol%, the obtained FeCu33 and FeCu50 show only the reflections characteristic of monoclinic CuO structure, and their diffraction intensity increases with the CuO content, indicating the excessive CuO species in the Cu–Fe–O systems, which is supported by the chemical analysis result shown in Table 1.

FeCu15 sample was taken as being representative for the investigation of the thermal stability of the prepared CuO–Fe_2O_3 composite catalysts. Fig. 2 shows the XRD patterns of FeCu15 catalysts calcined at different temperatures. It is seen that the samples remain amorphous when the calcination temperature was below 400 °C. And the hematite Fe_2O_3 phase presented with a progressive increase in the relative intensity of the lines when the calcination temperature above 400 °C, indicating an increase of the crystallinity and the growth of particle size by the thermal treatment. The very weak diffractions characteristic of CuO structure at 35.6° and 38.8° (2θ) can also be observed when the catalysts calcined at 500 °C or above. The TG–DTA result of the FeCu15 precursor is shown in Fig. 3. The process of weight loss can be divided into three steps. The endothermic peak between 40 and 125 °C on DTA, accompanied by 6.5% of weight loss observed in this first step on TG curve, is attributed to the desorption of water (that may be physical or chemical adsorption on the interparticle surface of the sample or reside the mesopores). The second from 125 to 300 °C with a main weight loss of about 15%, accompanied with a strong exothermic peak at 228 °C, can be attributed to the decomposition of the surfactant and the combustion of carbon species. The third from 300 to 500 °C with small weight loss might correspond to the decomposition of surface hydroxyl groups of the sample, which is related to the presence of the crystalline phases observed in Fig. 2.

Figs. 4 and 5 depict the N_2 adsorption–desorption isotherms and the corresponding pore size distributions of the CuO–Fe_2O_3 catalysts with different CuO content and calcined at different temperature. The textual properties of the samples are listed in Table 2. The isotherms of all the prepared samples are of classical type IV, characteristic of mesoporous materials

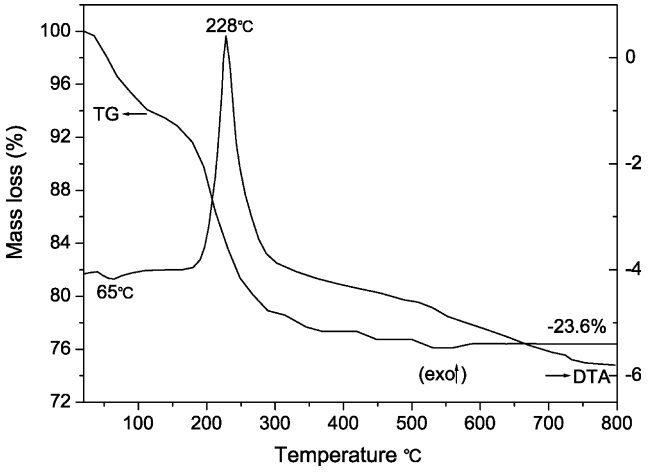

Fig. 3. TG–DTA patterns of the precursor of FeCu15 sample.

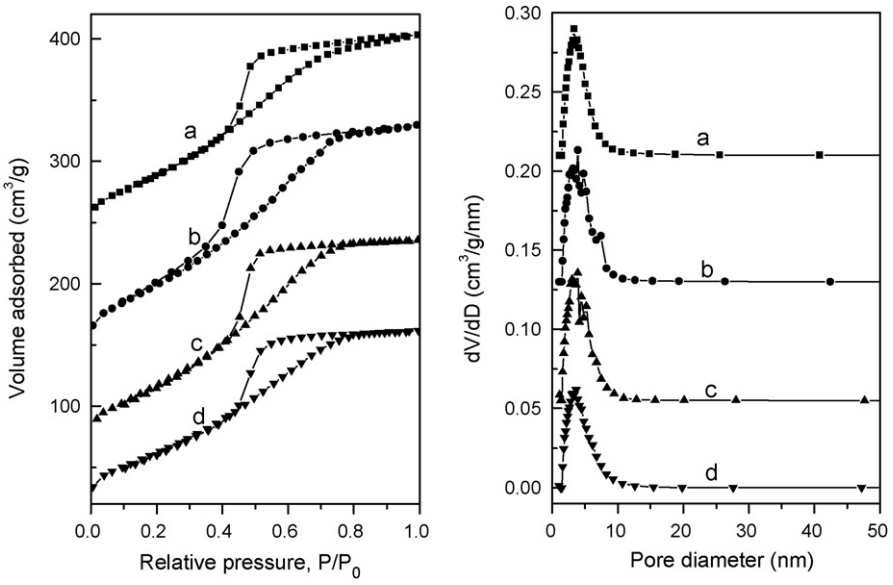

Fig. 4. (Left) N_2 adsorption–desorption isotherms and (right) the corresponding pore size distribution curves of the prepared CuO–Fe_2O_3 composite oxides with different CuO contents: (a) FeCu33, (b) FeCu20, (c) FeCu15 and (d) FeCu10. The volume was shifted by 220, 125 and 40 for the curves of data sets (a)–(c) and the d*V*/d*D* value was shifted by 0.21, 0.13 and 0.055 for the curves of data sets a–c, respectively.

according to the IUPAC. The well-defined hysteresis loops with a steep desorption branch and less steep adsorption branch belong to the H2-type, indicating that the effective radii of the mesoporous bodies are heterogeneously distributed and the effective radii of the narrow entrances are all of equal size [31]. The H2 type of the hysteresis loop is typical for wormhole-like mesostructures and hierarchical scaffold-like mesoporous structures formed by surfactant-assisted nanoparticle assembly [31,32]. The pore size distribution curves of the CuO–Fe_2O_3 catalysts with different CuO content after 300 °C-calcination, determined by the BJH method from the adsorption branch of the isotherms, exhibit one single narrow peak centered at 3.0–3.9 nm (Fig. 4), indicating the good homogeneity of the pores. With the increase of the CuO content from 15 to 50 mol%, the surface areas of these catalysts decreased from 299 to 200 m^2/g (Table 2), accompanied with the decrease of the pore volume. The pore size distributions of the FeCu15 catalysts calcined at different temperature are also narrow (Fig. 5), and the pore sizes enlarged with the increase of calcination temperature, accompanied with the decrease of the surface areas (due to the particle sintering) (Table 2). Interestingly, high surface area of 57 m^2/g can still be obtained after calcination at 500 °C for 5 h, indicating the high thermal stability of these surfactant-assisted synthesized CuO–Fe_2O_3 catalysts.

Such a uniform mesoporosity in these CuO–Fe_2O_3 composite catalysts determined by the N_2-sorption analysis

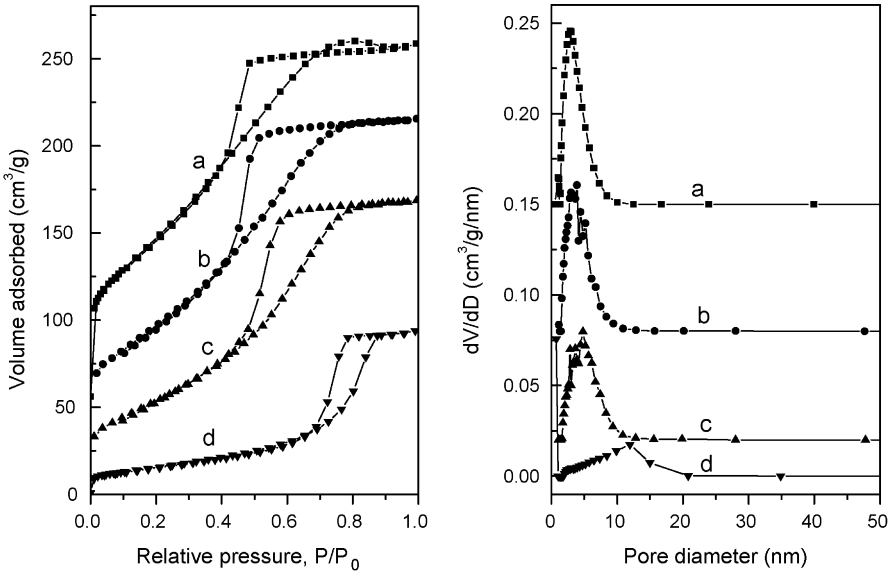

Fig. 5. (Left) N_2 sorption–desorption isotherms and (right) the corresponding pore size distribution curves of the FeCu15 samples calcined at different temperature: (a) 200 °C, (b) 300 °C, (c) 400 °C and (d) 500 °C. The volume was shifted by 55 and 20 for the curves of data sets a and b and the d*V*/d*D* value was shifted by 0.15, 0.08 and 0.02 for the curves of data sets (a)–(c), respectively.

Table 2
Textural properties and catalytic activities of the as-prepared catalysts

Samples	Calcination temperature (°C)	Surface area[a] (m^2/g)	Pore volume[b] (cm^3/g)	$D_{BJH\text{-}ads}$[c] (nm)	Average pore diameter[d] (nm)	T_{100} (°C)
Fe_2O_3	300	151	0.367	2.5	9.7	270
FeCu10	300	236	0.250	3.4	4.2	120
FeCu15	300	299	0.302	3.3	4.1	110
FeCu20	300	291	0.317	3.2	4.3	115
FeCu25	300	268	0.284	3.0	4.2	120
FeCu33	300	266	0.283	3.4	4.3	125
FeCu50	300	200	0.248	3.9	5.0	125
FeCu15	200	349	0.315	2.8	3.6	115
FeCu15	400	201	0.261	4.8	5.2	130
FeCu15	500	57	0.145	11.9	10.1	210

[a] Multi-point BET surface area.
[b] Total pore volume at $P/P_0 = 0.99$.
[c] Maximum of BJH pore diameter as determined from the adsorption branch.
[d] Average pore diameter ($4V/A$).

was further confirmed by the TEM observation. Fig. 6 shows the TEM micrographs of the FeCu15 sample calcined at 300 °C. The images clearly demonstrate that the FeCu15 sample has a disordered wormhole-like mesopore structure, formed by the agglomeration of the uniform nanoparticles. The accessible pores are connected randomly, lacking discernible long-range order in the pore arrangement among the small particles, being in well agreement with the N_2 adsorption–desorption isotherms. The nanoparticles in the sample are of regular spherical morphology with the size around 3–4 nm.

In order to illuminate the surface composition of the studied metal oxides and to acquire detailed information on the chemical states of the cations and anions, X-ray photoelectron spectroscopy was performed. Fig. 7a shows the general survey spectrum of the FeCu15 sample after 300 °C-calcination, which reveals that the surface of the sample contain Fe, Cu, O and C elements. The existence of C element may be caused by the coke residua after surfactant decomposition and/or surface-absorbed organic contaminant. Fig. 7b–d show the high-resolution XPS spectra of Cu 2p, Fe 2p and O 1s regions. In Fig. 7b, the XPS peak centered at about 954.1 and 934.5 eV correspond to Cu $2p_{1/2}$ and Cu $2p_{3/2}$, respectively. It has been well established that the presence of shake-up peak and a higher Cu $2p_{3/2}$ binding energy are two major XPS characteristics of CuO [33]. In the case of our study, the Cu $2p_{3/2}$ peak present at high binding energy (about 934.5 eV), along with the shake-up satellite peaks (about 940–944 eV), indicates the presence of Cu^{2+} species in the FeCu15 sample. The Fe 2p spectrum (Fig. 7c) displays the main peaks of Fe $2p_{3/2}$ and Fe $2p_{1/2}$ at the binding energies of 710.9 and 724.8 eV, respectively, together with a very weak satellite structure between the spin–orbit doublet. These parameters correspond to the Fe^{3+} surface species in α-Fe_2O_3 [34], indicating that iron is at the +3 state in the samples. The O 1s region (Fig. 7d) can be deconvoluted into two peaks at about 529.7 and 531.1 eV, which indicates the existence of two different oxygen species. It has been revealed that the first peak in the 529.5–530.5 eV range is the O 1s peak that characterizes the "O^{2-}" ions of the lattice oxygen, and the second peak in the range of 531.0–532.0 eV denotes O 1s lateral structure. This lateral peak corresponds to the ionizations of weakly adsorbed species and also the ionizations of oxygen ions with particular coordinations, more specifically integrated in the subsurface, suggesting the existence, in the subsurface, of oxygen ions with lower electron density, described as "O^-" species or excess oxygen [35,36].

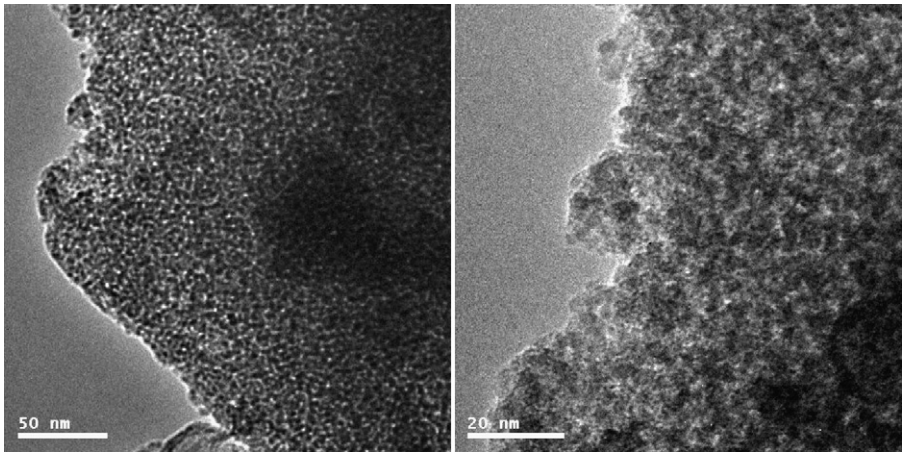

Fig. 6. TEM images of FeCu15 sample calcined at 300 °C.

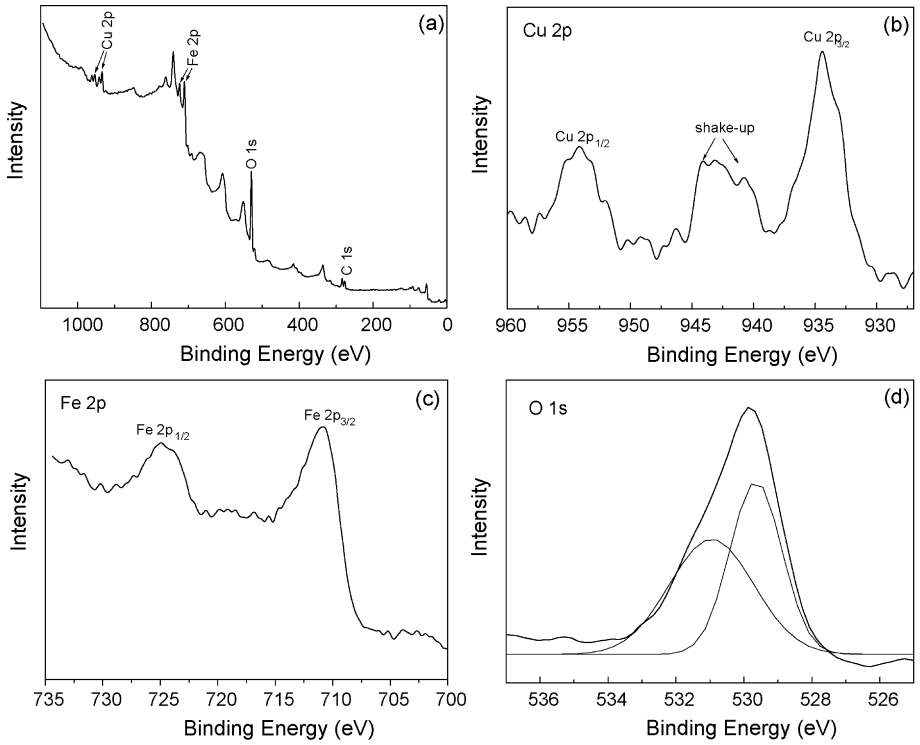

Fig. 7. XPS analysis of FeCu15 catalyst: (a) the general scan of the FeCu15 catalyst, (b) Cu 2p spectrum, (c) Fe 2p spectrum and (d) O 1s spectrum.

The XPS analysis also reveals that the surface atomic contents of Cu, Fe and O are 9.05, 29.13 and 61.82% for FeCu15 sample, respectively. The value of surface atomic ratio of Cu/(Cu + Fe) is 0.237, which is higher than the actual one (0.164) determined by the chemical analysis. This suggests that the CuO particles are mainly well dispersed on the surface of the catalyst.

H_2-TPR experiments were performed to get information about redox properties of the prepared samples. Fig. 8 shows the typical H_2-TPR profiles of FeCu15 calcined at 300 °C, and the reduction profile of pure Fe_2O_3 and CuO powder is also presented for comparison. The reduction of pure iron oxide starts at about 200 °C, and shows three peaks at around 358, 550 and 750 °C. The sharp peak at around 358 °C is associated with the reduction of Fe_2O_3 into magnetite Fe_3O_4, while the broad peaks at around 550 and 750 °C with large H_2 consumption amount are due to the subsequent multiple reduction of Fe_3O_4 to FeO and Fe [22,37]. TPR curve of pure CuO shows a single peak of maximum hydrogen consumption at about 346 °C. Whilst the FeCu15 sample shows three strong reduction peaks (A, B and C) at about 177, 212 and 650 °C, respectively. Compared with the pure iron oxide, the higher temperature peak (C in FeCu15 sample) corresponding to the multiple reduction of Fe_3O_4 to Fe is shifted from 750 to 650 °C, revealing that CuO lowered the reduction temperature of Fe_3O_4 to FeO and Fe. Several groups have reported that there are two reduction peaks for supported copper species [38,39], and these two reduction peaks are lower than the pure CuO. In the case of our study, the temperature reduction peaks (A and B) of copper species in the FeCu15 were also much lower than the pure CuO. This may be due to the synergistic effects between CuO and Fe_2O_3; Fe_2O_3 is promoting the reduction of CuO. The lower temperature peak A for FeCu15 could be ascribed to the reduction of finely dispersed CuO species on the catalyst surface, which are regarded as the active sites for CO oxidation. Since the possible incorporation of Cu^{2+} into the Fe_2O_3 lattice to form the CuO–Fe_2O_3 solid solution was suggested from the XRD results, and the occurrence of the reduction temperature shift to lower temperature due to an interaction between catalyst and support [40], the reduction peak B might be assigned to the reduction of Cu^{2+} species incorporated into the Fe_2O_3 lattice and/or related to the reduction of Fe_2O_3 to Fe_3O_4.

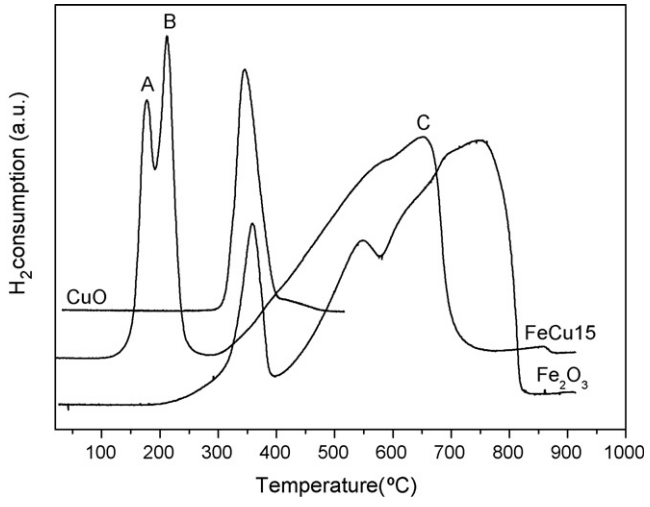

Fig. 8. H_2-TPR profiles of CuO, Fe_2O_3 and FeCu15 samples calcined at 300 °C.

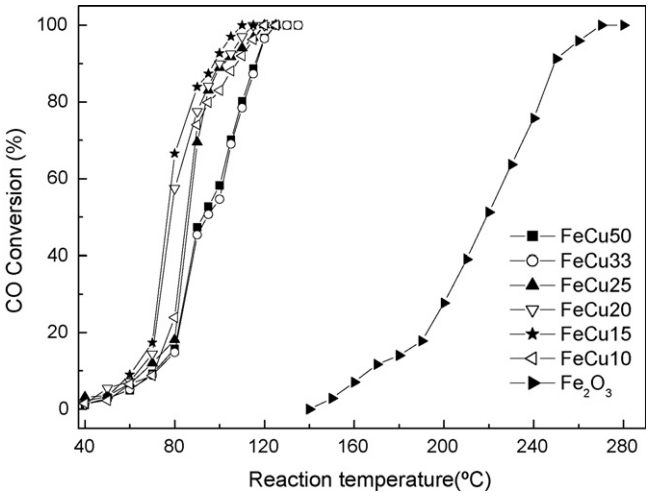

Fig. 9. Catalytic activity of mesoporous CuO–Fe_2O_3 catalysts with different CuO contents calcined at 300 °C for CO oxidation.

3.2. Catalytic activity

The variation of catalytic activity of the prepared mesoporous CuO–Fe_2O_3 composite catalysts for low-temperature CO oxidation as a function of reaction temperature were investigated and the results are shown in Figs. 9 and 10. All the catalysts present a similar behavior that the CO oxidation activity increased with the catalytic reaction temperature. The T_{100} (the temperature when the conversion is 100%) of the samples in the present reaction condition are shown in Table 2.

Fig. 9 presents the catalytic activity of mesoporous CuO–Fe_2O_3 composite catalysts with different content of CuO calcined at 300 °C, together with the catalytic activity of pure Fe_2O_3 for comparison purpose. It is seen that the activity of pure Fe_2O_3 is quite low, while the activities of all the mesoporous CuO–Fe_2O_3 catalysts are much higher than that of pure Fe_2O_3. The pure CuO had no activity under the present condition. This illuminates that there is a synergistic effect between CuO and Fe_2O_3, which strongly affect the catalytic activity in low-temperature CO oxidation. The catalytic activity of mesoporous CuO–Fe_2O_3 catalysts enhanced with the increase of CuO content from 10 to 15 mol%, but decreased with the further increase of CuO content. The FeCu15 catalyst, that has the highest surface area of 299 m^2/g, exhibited the highest catalytic activity. It is well reported that the high specific surface area of nanostructured catalysts results in more unsaturated surface coordination sites exposed to the reaction gas [24,41] so as to enhance the catalyst activity. The higher surface area and narrower mesopore size distribution could promote the formation of higher dispersion of metal or oxide catalyst nanoparticles giving thus some beneficial effect on the catalytic performance. Whereas, when the high loading of CuO, the excess CuO species would not only cover some of the active sites, but also lead the grown CuO particles or bulk CuO formation, which maybe have negative effect on the catalytic activity of low-temperature CO oxidation.

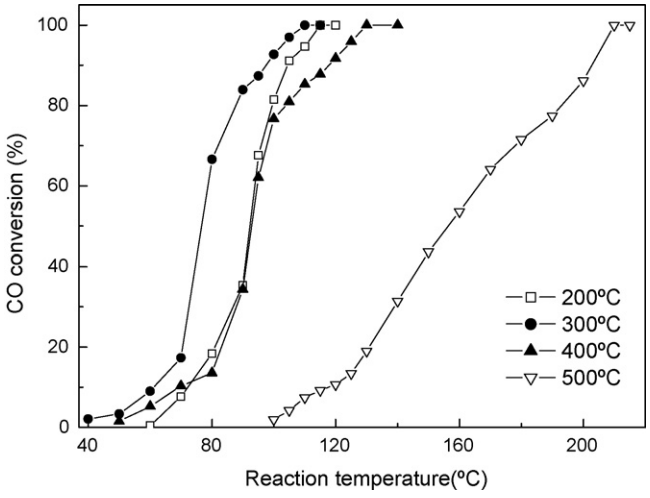

Fig. 10. Catalytic activity of FeCu15 samples calcined at different temperatures for CO oxidation.

Fig. 10 illustrates the catalytic performance of FeCu15 samples calcined at different temperature for CO oxidation. The catalytic activity of the FeCu15 catalysts increased with the increase of precalcination temperature from 200 to 300 °C, but decreased from 300 to 500 °C. FeCu15 catalyst calcined at 300 °C, which has the high surface area of 299 m^2/g and the particle size of 3–4 nm (measured by TEM), exhibits the highest catalytic activity on CO oxidation with CO total conversion at 110 °C. The 500 °C-calcined FeCu15 catalyst having the lowest surface area of 57 m^2/g with large particle size of 25.8 nm (calculated by the Scherrer formula), presents T_{100} at 210 °C, which is the lowest one in all the composite catalysts we studied. The XRD and nitrogen adsorption–desorption analysis has revealed that the heat treatment made the decrease of the surface areas, the increase of the pore sizes and the particle sizes with the increase of calcination temperatures. Thus, the observed difference in the catalytic activities of the FeCu15 catalysts calcined at different temperature maybe due to the agglomeration of the catalysts, the decrease of the surface areas, and the increase of the particle sizes by the increase of the calcination temperature. It is believed that high activity of these CuO–Fe_2O_3 catalysts is corresponding to their high mesoporosity. The mesoporous frameworks provide a large surface to volume ratio, and hence more active sites are available for CO oxidation, benefiting to the enhanced catalytic activity.

In order to investigate the influence of space velocity on the catalytic activity of the mesoporous CuO–Fe_2O_3 composite catalysts, the activities of CO oxidation over FeCu15 catalyst at different WHSVs were tested (Fig. 11a). It can be seen that T_{100} (160 °C) is higher at high WHSV (60,000 ml/(h g)) than at low WHSV (11,000 ml/(h g)), which may be due to the contact time with the catalysts at high WHSV is lower than that at low WHSV. The FeCu15 catalyst was also selected as representative to investigate the stability of the prepared mesoporous catalysts. Fig. 11b displays the variation of the catalytic activity of the 300 °C-calcined FeCu15 catalyst at high WHSV (60,000 ml/(h g)) for low-temperature CO oxidation as a function of reaction time, where the reaction temperature was maintained at 160 °C (T_{100}) and 130 °C (T_{50}: the temperature

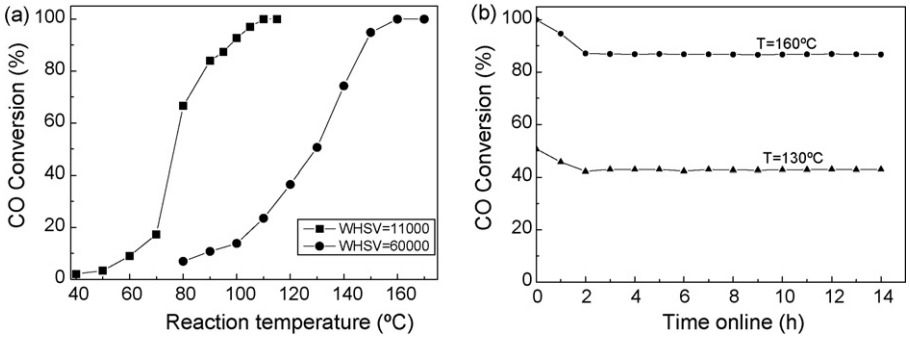

Fig. 11. (a) The influence of space velocity on the catalytic activity of FeCu15 samples calcined at 300 °C and (b) the stability testing of FeCu15 catalyst for CO oxidation performed at the WHSV = 60,000.

when the conversion of CO is 50%). It is found that the catalyst showed a decrease in catalytic activity over first 2 h, but after this period the activity changed very slightly and maintained high activity (the conversion of CO was about 87% at 160 °C and 42% at 130 °C, respectively) over 14 h during the period of reaction. Cheng et al. [26] reported that the initial deactivation may be resulted from the interaction between the reactants and oxides, through which redox balance and stable surface composition were established in the initial stage. This stability test experimental result demonstrates that these mesoporous $CuO–Fe_2O_3$ catalysts are stable on low-temperature CO oxidation.

Compared with the reported Au-based catalysts in the literature [15–22], the activity of our prepared $CuO–Fe_2O_3$ catalysts is relative low, but comparable to the reported CuO-based catalysts [24]. Since the components copper and iron in $CuO–Fe_2O_3$ catalysts are very cheaper than precious metal catalysts, on the viewpoint of the relationship of cost and activity, the present mesoporous $CuO–Fe_2O_3$ composite catalysts system is worthy of further investigation.

4. Conclusions

Mesoporous $CuO–Fe_2O_3$ composite catalysts with high catalytic activity and stability for low-temperature carbon monoxide oxidation have been prepared by the surfactant-assisted method of nanoparticle assembly. The observed high catalytic activity is related to the structural features of wormhole-like mesoporous structure with narrow pore size distribution, high BET surface area, uniform distribution of CuO particles with nanoscale size, and high thermal stability. The content of CuO and the precalcination temperature can also affect the catalytic properties of the catalysts remarkably. The FeCu15 catalyst calcined at 300 °C, which is of amorphous nature and has the highest surface area, exhibits the highest catalytic activity of the total CO oxidation temperature at 110 °C. These mesoporous $CuO–Fe_2O_3$ materials may find other applications such as in gas purification and carbon monoxide gas sensor.

Acknowledgements

This work was supported by the National Natural ScienceFoundation of China (nos. 20473041 and 20673060), the National Basic Research Program of China (no. 2003CB615801), the Chinese-Bulgarian Scientific and Technological Cooperation Project, the MOE Supporting Program for New Century Excellent Talents (NCET-06-0215), and Nankai University.

References

[1] C. Suryanarayana, C.C. Koch, Non-Equilibrium Processing of Materials; Pergamon Materials Series, Pergamon Press, New York, 1999.
[2] Z.Y. Yuan, B.L. Su, J. Mater. Chem. 16 (2006) 663.
[3] H. Zeng, P.M. Rice, S.X. Wang, S. Sun, J. Am. Chem. Soc. 126 (2004) 11458.
[4] T.Z. Ren, Z.Y. Yuan, A. Azioune, J.J. Pireaux, B.L. Su, Langmuir 22 (2006) 3886.
[5] Z.Y. Yuan, T.Z. Ren, A. Azioune, J.J. Pireaux, B.L. Su, Chem. Mater. 18 (2006) 1753.
[6] S. Velu, M.P. Kapoor, S. Inagaki, K. Suzuki, Appl. Catal. A 245 (2003) 317.
[7] V. Idakiev, T. Tabakova, A. Naydenov, Z.Y. Yuan, B.L. Su, Appl. Catal. B 63 (2006) 178.
[8] Z.Y. Yuan, T.Z. Ren, B.L. Su, Catal. Today 93–95 (2004) 743.
[9] U. Schwetmann, R.M. Cronell, Iron Oxides in the Laboratory, VCH, New York, 1991.
[10] S.S. Lin, M.D. Gurol, Environ. Sci. Technol. 32 (1998) 1417.
[11] J. Chen, L.N. Xu, W.Y. Li, X.L. Gou, Adv. Mater. 17 (2005) 582.
[12] Y. Wang, S.R. Wang, Y.Q. Zhao, B.L. Zhu, F.H. Kong, D. Wang, S.H. Wu, W.P. Huang, S.M. Zhang, Sens. Actuators B 125 (2007) 79.
[13] Y. Wang, F.H. Kong, B.L. Zhu, S.R. Wang, S.H. Wu, W.P. Huang, Mater. Sci. Eng. B 140 (2007) 98.
[14] Y.H. Zheng, Y. Cheng, Y.S. Wang, F. Bao, L.H. Zhou, X.F. Wei, Y.Y. Zhang, Q. Zheng, J. Phys. Chem. B 110 (2006) 3093.
[15] M. Haruta, N. Yamada, T. Kobayashi, S. Iijima, J. Catal. 115 (1989) 301.
[16] M. Haruta, S. Tsubota, T. Kobayashi, H. Kageyama, M.J. Genet, B. Delmon, J. Catal. 144 (1993) 175.
[17] N.A. Hodge, C.J. Kiely, R. Whyman, M.R.H. Siddiqui, G.J. Hutchings, Q.A. Pankhurst, F.E. Wagner, R.R. Rajaram, S.E. Golunski, Catal. Today 72 (2002) 133.
[18] G.J. Hutchings, M.S. Hall, A.F. Carley, P. Landon, B.E. Solsona, C.J. Kiely, A. Herzing, M. Makkee, J.A. Moulijn, A. Overweg, J.C. Fierro-Gonzalez, J. Guzamn, B.C. Gates, J. Catal. 242 (2006) 71.
[19] M. Khoudiakov, M.C. Gupta, S. Deevi, Nanotechnology 15 (2004) 987.
[20] G.J. Hutchings, Catal. Today 100 (2005) 55.
[21] S. Al-Sayari, A.F. Carley, S.H. Taylor, G.J. Hutchings, Top. Catal. 44 (2007) 123.
[22] M. Khoudiakov, M.C. Gupta, S. Deevi, Appl. Catal. A 291 (2005) 151.
[23] P. Landon, J. Ferguson, B.E. Solsona, T. Garcia, A.F. Carley, A.A. Herzing, C.J. Kiely, S.E. Golunski, G.J. Hutchings, Chem. Commun. 27 (2005) 3385.

[24] J.-L. Cao, Y. Wang, T.-Y. Zhang, S.-H. Wu, Z.-Y. Yuan, Appl. Catal. B 78 (2008) 120.
[25] M. Manzoli, R. Di Monte, F. Boccuzzi, S. Coluccia, J. Kašpar, Appl. Catal. B 61 (2005) 192.
[26] T. Cheng, Z.Y. Fang, Q.X. Hu, K.D. Han, X.Z. Yang, Y.J. Zhang, Catal. Commun. 8 (2007) 1167.
[27] H.G. El-Shobaky, M.M. Mokhtar, Appl. Surf. Sci. 253 (2007) 9407.
[28] H.G. El-Shobaky, Y.M. Fahmy, Mater. Res. Bull. 41 (2006) 1701.
[29] W.M. Shaheena, A.A. Ali, Int. J. Inorg. Mater. 3 (2001) 1073.
[30] E. Boellaard, F.Th. van de Scheur, A.M. van de Kraan, J.W. Geus, Appl. Catal. A 171 (1998) 333.
[31] Z.Y. Yuan, B.L. Su, Chem. Phys. Lett. 381 (2003) 710.
[32] T.Z. Ren, Z.Y. Yuan, B.L. Su, Chem. Phys. Lett. 374 (2003) 170.
[33] G. Avgouropoulos, T. Ioannides, Appl. Catal. A 244 (2003) 155.
[34] M. Sorescu, R.A. Brand, D. Mihaila-Tarabasanu, L. Diamandescu, J. Appl. Phys. 85 (1999) 5546.
[35] J.C. Dupin, D. Gonbeau, P. Vinatier, A. Levasseur, Phys. Chem. Chem. Phys. 2 (2000) 1319.
[36] W. Cao, O.K. Tan, J.S. Pan, W. Zhu, C.V.G. Reddy, Mater. Chem. Phys. 75 (2002) 67.
[37] G. Munteanu, L. Ilieva, D. Andreeva, Thermochim. Acta 291 (1997) 171.
[38] Lj. Kundakovic, M. Flytzani-Stephanopoulos, Appl. Catal. A 171 (1998) 13.
[39] P. Ratnasamy, D. Srinivas, C.V.V. Satyanarayana, P. Manikandan, R.S.S. Kumaran, M. Sachin, V.N. Shetti, J. Catal. 221 (2004) 455.
[40] A. Venugopal, M.S. Scurrell, Appl. Catal. A 258 (2004) 241.
[41] L.X. Yin, Y.Q. Wang, G.S. Pang, Y. Koltypin, A. Gedanken, J. Colloid Interface Sci. 246 (2002) 78.